



Review

Impact of biodiesel impurities on carbon oxidation in passive regeneration conditions: Influence of the alkali metals



Julie Schobing, Valerie Tschamber*, Alain Brillard, Gontrand Leyssens

Université de Haute-Alsace, LGRE (Laboratoire Gestion des Risques et Environnement) EA2334, F-68093 Mulhouse, France

ARTICLE INFO

Keywords:
 Soot
 Biodiesel impurities
 Alkali metals
 Phosphorus
 Passive regeneration

ABSTRACT

Soot model (Carbon Black (CB)) were impregnated by Na, K or P in aqueous solution, to simulate the poisoning process of soot by biodiesel impurities. Oxidation of non-doped and doped CB samples was performed under Temperature Programmed Oxidation (TPO) and under different oxidizing atmospheres containing NO₂ to simulate passive regeneration conditions. Active regeneration conditions were tested through thermogravimetric analyses (TGA). Alkali metals exhibit a beneficial effect on the oxidation process through the whole temperature range, regardless the reactive gas flow. Phosphorus has a beneficial effect on C-NO₂ reaction, particularly in presence of water, but inhibits the C-O₂ reaction. Characterizations of the samples through elemental analysis, X-Ray Photoelectron Spectroscopy (XPS), nitrogen adsorption and Raman spectroscopy prove that alkali metals increase the specific surface area of CB samples and lead to a decrease in their internal structure order. Impregnation of CB samples by phosphorus leads to a decrease in specific surface area and to a greater organization of the carbon structure. The kinetic constants which are derived through numerical simulations prove that the higher reactivity of doped CB samples is linked to a decrease in activation energy of both C-NO₂ and C-O₂-NO₂ reactions and an increase in the number of active sites.

1. Introduction

To comply with the European Directive 2009/28/CE promoting renewable energies [1] and Euro VI emission standards [2], car and truck manufacturers have to replace more and more conventional Diesel by Biodiesel. The use of Biodiesel as car fuel has globally a positive impact on pollutant emissions, as it reduces the overall carbon footprint and soot production [3,4]. Biodiesel is obtained by transesterification of triglycerides contained in vegetable oils or animal fats [3]. It is characterized by its high oxygen content and the presence of inorganic elements like alkali metals, phosphorus... [3,5]. Although the concentration of each of these elements in Biodiesel is limited by EN 14214 standards [6], the use of large amounts of Biodiesel on long distances may lead over time to an important deposit of inorganic elements on the whole depollution car system [7]. Inorganic elements may thus interact with the different catalysts and thus modify their activity. It is known that these inorganic elements have a negative impact on Diesel Oxidation Catalyst (DOC) and Selective Catalytic Reduction (SCR) devices, because of the occurrence of poisoning active sites [7,8]. In the Diesel Particulate Filter (DPF), inorganic elements can be found on the monolith wall but also in the soot composition or as ash [7,9].

Previous studies proved that catalysts containing alkali metals have a stronger activity regarding soot oxidation by O₂ [10–16]. Studying the carbon black (CB) oxidation in presence of MgO in tight contact under air, Jiménez et al. [11,12] proved that catalyst doped with 5 wt% of KNO₃ leads to a shift of the maximum oxidation peak by 200 °C to lower temperatures. They explained this reactivity increase by the decrease in the activation energy associated to the C-O₂ reaction because of potassium. Gross et al. [13] studied the CB oxidation under air on ceria catalysts doped by different KNO₃ contents (4–14 wt%). According to their results, K enhances carbon oxidation through the improvement of the contact between catalyst and soot because of its high mobility. Other authors also proved that, beyond 7 wt% of K, no more beneficial impact on carbon oxidation is observed. Aneggi et al. [14] studied the impact of different concentrations (3–13,5 wt%) of four alkali metals (Na, K, Rn and Cs) on CeO₂ activity. It has been proved that, whatever the inorganic element, a concentration of 10 wt% allows the highest catalytic impact on carbon oxidation under air. Between the four alkali metals, cesium exhibits the highest activity. Matarrese et al. [15] and Castoldi et al. [16] highlighted the intrinsic activity of alkali metals. They indeed proved that Na, K and Cs have a catalytic impact on carbon oxidation under air, whatever their impregnation on a catalyst support (alumina) or directly on CB. Cs and K even possess a better

* Corresponding author.

E-mail address: valerie.tschamber@uha.fr (V. Tschamber).

reactivity than noble metals like Pt. On the contrary, few studies reveal that phosphorus, which can also be found in Biodiesel fuel, presents an inhibiting impact on the C-O₂ reaction [17–20]. Thus inorganic elements contained in fossil Diesel soot can change the CB reactivity under air and so the active regeneration of DPF. Surprisingly, the impact of inorganic element on carbon oxidation in presence of NO₂ in the feed gas is not reported in the literature. However, soot oxidation with NO₂ as oxidant agent plays a fundamental role in the regeneration of the DPF, as it is carried out continuously and participates to a great extent in the oxidation of soot when the temperature of the exhaust gases is low (< 450 °C).

Several studies proved that Biodiesel soot are more reactive than Diesel soot [10,21,22]. The better reactivity of Biodiesel soot has been attributed to their more amorphous structure [21,22], but also to their higher oxygen content and the presence of alkali metals [10].

The aim of the present work is to evaluate the impact of the presence of inorganic compounds in Biodiesel composition on the DPF passive regeneration, i.e. using NO₂ as oxidizing reagent. To this end, the oxidation behavior, under several gas mixtures containing NO₂, of model soot (CB) doped by 0.5 wt% of inorganic elements which may be found in Biodiesel fuels: Na, K and P, has been studied. These concentrations intend to represent that of Biodiesel soot.

Numerical simulations of the oxidation mechanism were performed in order to evaluate the impact of inorganic elements on the values of the kinetic constants associated to the oxidation reactions.

2. Experimental conditions

2.1. Doping procedure

Carbon Black Vulcan 6 (CB) was used as model soot. CB doping was performed through incipient wetness, the powder being impregnated by an aqueous solution of NaNO₃, KNO₃ or (NH₄)₂PO₄ under agitation and heating until the water was evaporated. Then the sample was dried at 110 °C for a night and calcined in a muffle furnace at 350 °C for 2 h. Such samples will be noted CB-0,5X, X being the symbol of the inorganic element.

Undoped CB samples which have only undergone the calcination step are taken as reference. They are noted CB350.

2.2. Reactivity test

Thermogravimetric Analyses (TGA) were performed on a TA Q500 thermobalance under air from room temperature up to 700 °C. All TGA were performed with about 5 mg of soot and under a heating ramp of 5 °C/min.

Soot reactivity under passive regeneration conditions was studied performing Temperature Programmed Oxidation (TPO) tests under different atmospheres: 400 ppmv NO₂ in N₂, 400 ppmv NO₂ + 10% b.v. O₂ in N₂, 400 ppmv NO₂ + 10% b.v. H₂O in N₂ or 400 ppmv NO₂ + 10% b.v. O₂ + 10% b.v. H₂O in N₂. Gas mixtures containing only NO₂ as nitrogen oxide were used as it is assumed that nowadays vehicles exhaust line consists of a Diesel oxidation catalyst (DOC) placed up-stream the DPF. A large part of the NO formed in the engine is also converted into NO₂ on the DOC. Moreover, it is known that NO has no activity with respect to soot oxidation reactions during the passive regeneration of the DPF.

TPOs were performed using a tubular fixed bed reactor (internal diameter 16 mm). All gases were injected via different mass flow meters (Brooks 5850S and Brooks Delta II). The water vapor was introduced using a liquid mass flow meter (Brooks Flomega 5881) followed by an evaporator. The total flow rate through the reactor was 90 NL/h. The temperature was measured by a thermocouple (K-type) located within the catalyst bed. 15 mg of carbon sample were diluted in 200 mg of SiO₂ to avoid heat transfer and reactor clogging. Reactive gas flow was injected at ambient temperature. Then temperature was increased up to

700 °C under a 5 °C/min temperature ramp. The outlet gases were analyzed using an infrared Rosemount Xstream analyzer to quantify the outlet NO, NO₂, CO and CO₂ molar fractions.

From each experiment, the carbon specific oxidation rate (V_{spe} in mg/s/g_{cini}) was calculated from CO and CO₂ emissions (X_{CO} and X_{CO₂} in ppmv) through:

$$V_{spe} = \frac{(X_{CO} + X_{CO_2}) * D * M_C}{10^{6*3600} * V_M * m_{cini}}$$

where V_{spe} is expressed per gram of carbon initially introduced in the reactor (m_{cini}), D corresponds to the flow rate in NL/h and V_M is the molar volume (V_M = 22.4 l/mol).

2.3. Characterizations

Elemental composition of Carbon, Hydrogen, Oxygen, Nitrogen and Sulfur of the different samples was measured by CHONS (note that Oxygen content was measured and not calculated through mass balance). Flame Atomic Absorption Spectroscopy (FAAS) after microwave digestion at 260 °C with HF (1 ml/50 mg), H₂SO₄ (5 ml/50 mg), HCl (1 ml/50 mg) and HNO₃ (1 ml/50 mg), was used for alkali metals (Na and K) and Inductively Coupled Plasma-Optical Emission Spectroscopy (ICP-OES), after a first microwave digestion (rate 10 °C/min up to 180 °C then 180 °C during 20 min) with HF (4 ml/100 mg), then a second one with the addition of HNO₃ (3 ml), for phosphorus content (P).

The textural properties such as specific surface area, micropore surface area and micropore volume are determined by N₂ adsorption-desorption isotherms which are obtained using Micromeritics ASAP2020 apparatus. BET method was used to calculate surface specific area and t-plot method for microporous volume.

XPS analyses were performed on a VG SCIENTA SES-2002 equipped with a hemispherical analyzer and a RX source generating a monochromatic Al K_{α1,2} radiation (1486.6 eV). Emited electrons were collected using a takeoff angle of 90° and detected by an analyzer operating at constant pass energy of 100 eV in the fixed transmission mode. The power of the RX radiation source is 420 W and the base pressure in the analysis chamber was about 10⁻⁹ mbar. The analyzed surface area was approximately 6 × 0.5 mm². The spectrometer energy scale was calibrated using the Au4f^{7/2}, Ag3d^{5/2}, and Cu2p^{3/2} peaks respectively corresponding at binding energies of 84.00, 368.20 and 932.70 eV. All spectra were referenced compared to C1 s peak at 285.00 eV. The CasaXPS software was used for data treatment.

XPS analyses were only performed on CB-0,5Na and CB-0,5P. In fact, in the present context, a potassium concentration equal to 0.5 wt% does not allow the distinction between K peak (BE ~ 293 eV) and C peak (284 eV < BE < 292 eV) [23].

Raman spectra were recorded on a Horiba Labram 300 apparatus using a 532 nm laser. A scanning range of 2200 cm⁻¹ was chosen. The spectrometer includes a grating with 600 grooves/mm and a CCD detector with 50 x magnification objective lens. Decomposition of the spectra was done according to the Sadezky et al. [24] method.

2.4. Modelling

The model which has been used to extract the kinetic constants is based on a model developed in previous works [25–27], initially developed for an isothermal condition, but here adapted to ramp temperature conditions of TPO experiments. As the model only considers passive regeneration conditions, it was applied on the temperature range 150 – 450 °C. It has been verified performing a blank experiment that until 500 °C no NO₂ is spontaneously converted into NO. As kinetic modeling also only focused on temperatures lower than 450 °C, the NO/NO₂ equilibrium was not included in the model.

The bed, which lies between 0 and *h* > 0, is decomposed in *N_z* thin

layers of equal thinness $dz = h/N_z$.

Based on the global mechanism proposed by Jacquot et al. in [24], the following empirical kinetic law for soot oxidation by NO_2 in the presence of O_2 is written as:

$$-\frac{1}{\delta m} \frac{d(\delta m)}{dt} = k_{\text{CO}_2} P_{\text{NO}_2} + k_{\text{CO}} P_{\text{NO}_2} + (k_{\text{O}_2\text{CO}_2} P_{\text{NO}_2} X_{\text{O}_2}^{0.3} + k_{\text{O}_2\text{CO}} P_{\text{NO}_2} X_{\text{O}_2}^{0.3}), \quad (1)$$

where: $-\delta m$ is the local soot mass (kg),

- k_{CO_2} , k_{CO} , $k_{\text{O}_2\text{CO}_2}$ and $k_{\text{O}_2\text{CO}}$ are the kinetic constants ($\text{Pa}^{-1}\cdot\text{s}^{-1}$) which have to be determined,
- P_{NO_2} is the local partial NO_2 pressure (Pa) defined as $P_{\text{NO}_2} = X_{\text{NO}_2} P_{\text{tot}}$, where X_{NO_2} is the NO_2 mole fraction and P_{tot} is the total pressure in the fixed bed reactor: $P_{\text{tot}} \approx 1,2 \times 10^5 \text{ Pa}$.

In each layer of the bed, the balance for each gaseous species leads to the following equations:

$$\begin{cases} \frac{\partial X_{\text{NO}_2}}{\partial z}(z, t) = -\frac{V_m}{D_V}(T) \frac{2r_1+r_2+r_3+r_4}{M_c} X_{\text{NO}_2}(z, t) m(z, t), \\ \frac{\partial X_{\text{NO}}}{\partial z}(z, t) = \frac{V_m}{D_V}(T) \frac{2r_1+r_2+r_3}{M_c} X_{\text{NO}_2}(z, t) m(z, t), \\ \frac{\partial X_{\text{CO}_2}}{\partial z}(z, t) = \frac{V_m}{D_V}(T) \frac{r_1+r_3}{M_c} X_{\text{NO}_2}(z, t) m(z, t), \\ \frac{\partial X_{\text{CO}}}{\partial z}(z, t) = \frac{V_m}{D_V}(T) \frac{r_2+r_4}{M_c} X_{\text{NO}_2}(z, t) m(z, t), \end{cases} \quad (2)$$

with $r_1 = k_{\text{CO}_2} P_{\text{tot}}$, $r_2 = k_{\text{CO}} P_{\text{tot}}$, $r_3 = k_{\text{O}_2\text{CO}_2} P_{\text{tot}} X_{\text{O}_2}^Y$, $r_4 = k_{\text{O}_2\text{CO}} P_{\text{tot}} X_{\text{O}_2}^Y$.

The system (1) – (2) is completed with the following initial conditions:

$$\begin{aligned} X_{\text{NO}_2}(z, 0) &= 0, 0, & X_{\text{CO}_2}(z, 0) &= 0, 0, \\ X_{\text{NO}}(z, 0) &= 0, 0, & X_{\text{CO}}(z, 0) &= 0, 0, \\ m(z, 0) &= \frac{m_0}{N_z}, \end{aligned} \quad (3)$$

where m_0 is the initial soot mass contained in the bed.

The boundary conditions at the entrance of the bed ($z = 0$) are:

$$\begin{aligned} X_{\text{NO}_2}(0, t) &= X_{\text{NO}_2,0}, & X_{\text{CO}_2}(0, t) &= 0, 0, \\ X_{\text{NO}}(0, t) &= 0, 0 & X_{\text{CO}}(0, t) &= 0, 0, \end{aligned} \quad (4)$$

where $X_{\text{NO}_2,0}$ represents the imposed NO_2 concentration at the entrance of the bed, which is a constant expressed in ppm and which depends on the experiments.

The problem (1) – (4) is solved using an explicit Euler method in an alternate way with initial values of the kinetic constants. An optimization procedure is used which consists to minimize the error between the experimental and simulated data for the different gases and for the remaining sample mass at regularly disposed computational times t_j . For example, under a NO_2 atmosphere, this error is taken as:

$$\text{error} = \sup \left(\begin{array}{l} |(X_{\text{NO}_2})_{\text{exp}}(t_j) - (X_{\text{NO}_2})_{\text{sim}}(t_j)|^2 \\ + \left| (X_{\text{CO}_2})_{\text{exp}}(t_j) - \left(\begin{array}{c} X_{\text{C}} \\ \text{O}_2 \end{array} \right)_{\text{sim}}(t_j) \right|^2 \\ + |m_{\text{exp}}(t_j) - m_{\text{sim}}(t_j)|^2 \end{array} \right).$$

In order to avoid possible kinetic compensation effects, the initial guess of the kinetic parameters have been chosen the same for the different samples: $A_{\text{CO}_2} = 2.5 \cdot 10^{-3}$; $E_{\text{aCO}_2} = 4.54 \cdot 10^4$; $A_{\text{CO}} = 1.3 \cdot 10^{-3}$; $E_{\text{aCO}} = 4.2 \cdot 10^4$, under a NO_2 atmosphere, and $A_{\text{O}_2\text{CO}_2} = A_{\text{CO}_2}$; $E_{\text{aO}_2\text{CO}_2} = E_{\text{aCO}_2}$; $A_{\text{O}_2\text{CO}} = A_{\text{CO}}$; $E_{\text{aO}_2\text{CO}} = E_{\text{aCO}}$, under a $\text{NO}_2 + \text{O}_2$ atmosphere.

Table 1

Elemental composition of the doped carbons black in wt% (${}^1\text{CHONS}$, ${}^2\text{AA}$, ${}^3\text{ICP}$, n.m. = non measured, n.d. = non detected).

Sample	C ¹	H ¹	O ¹	N ¹	S ¹	Na ²	K ²	P ³
CB [28]	95.3	0.7	n.m.	< 0.3	1.0	n.m.	n.m.	n.m.
CB350	91.5	0.23	3.31	0.10	0.73	0.01	0.01	n.d.
CB-0,5Na	88.7	0.44	5.15	0.13	0.97	0.55	n.d.	n.m.
CB-0,5 K	87.9	0.67	5.72	0.11	0.82	n.d.	0.48	n.m.
CB-0,5P	89.5	0.35	4.50	0.14	0.67	n.d.	n.d.	0.38

3. Results and discussion

3.1. Material characterization

The elemental composition of the different soot samples is presented in Table 1.

The model soot are naturally mainly composed of carbon. Less than 1% of hydrogen and nitrogen are found in the samples. For doped CB samples, the low content of N confirms the decomposition of the impregnation precursor during the calcination step. Doped CB samples possess higher oxygen content than CB350. This means that inorganic elements are present in an oxygenated form. CB350 and CB-0,5P contain 0.73 wt% and 0.67 wt% of sulfur, respectively. These concentrations are low in comparison with the initial sulfur content of CB before any treatment. It seems that a part of sulfur is lost during the calcination step. CB-0,5Na and CB-0,5 K present percentages of S close to the CB one [29]. It is possible that, in these samples, the presence of Na or K prevents this loss. Measurements of %Na and %K validate the impregnation procedure. In fact, the measured concentrations are close to the theoretical ones (0.5 wt%). Considering phosphorus, the measured concentrations is lower than expected. The impregnation seems to be less adapted for this element, probably because of its anion nature in comparison to Na and K.

The XP spectrum of the Na1 s energy region of the CB-0,5Na sample (Fig. 1) reveals that Na was only detected in a sulfate/sulfonate form (Na2s spectrum: BE = 1071.36 eV). This form is confirmed by the detection of S and O in SO_x form too (S2p spectrum: BE = 168.63 eV and 166.30 eV; O1s spectrum: BE = 531.55 eV) [23,30,31]. The global formula of sodium in CB-0,5Na is thus Na₂SO_x (with x = 3 or 4). In the case of CB-0,5Na, the lower loss of sulfur observed during the calcination step (Table 1) is likely due to the formation of Na₂SO_x.

XP spectra of CB-0,5P sample in the C1s, O1s, S2p and P2p energy region are presented in Fig. 2. Phosphorus was only detected in phosphate form (P2p energy region: BE = 133.71 eV) [17,18]. This form is confirmed by the detection of oxygen linked to P by single (O-P, O1s spectra: BE = 531.45 eV) and double bindings (O=P, O1s energy region: BE = 532.85 eV) [17]. Spectrum of C1s energy region does not show any evidence of C-P bindings in CB-0,5P [17,32,33]. So phosphates do not seem to be linked to the carbon surface via C-P bindings in the sample. Different authors [17–20,32,33] have already shown that phosphorus contained in activated carbon impregnated by phosphoric acid, is likely present in the form C-O-PO₃ or (CO)₃-P with C an atom of the carbon surface. C-O-P is hardly detectable by XPS because its binding energy is close to alcohol and ether groups which are also present on the doped Carbon Black surface [17,18,32]. It may be assumed that P on CB-0,5P is present in C-O-PO₃ or (CO)₃-P forms.

Quantitative analyses of CB-0,5Na and CB-0,5P surface composition were performed through XP spectroscopy. Results are given by Table 2. It can be observed that CB-0,5P surface contains 0,41 wt% of P. This value is close to the one measured by ICP-OES analysis (0,38 wt%). It seems that phosphorus is homogeneously distributed in CB-0,5P sample. On the other hand, only 0,29 wt% of Na were detected on CB-0,5Na surface against 0,55 wt% detected by bulk analyses (FAAS). In the case of CB-0,5Na, it seems that sodium is lesser present on the sample surface.

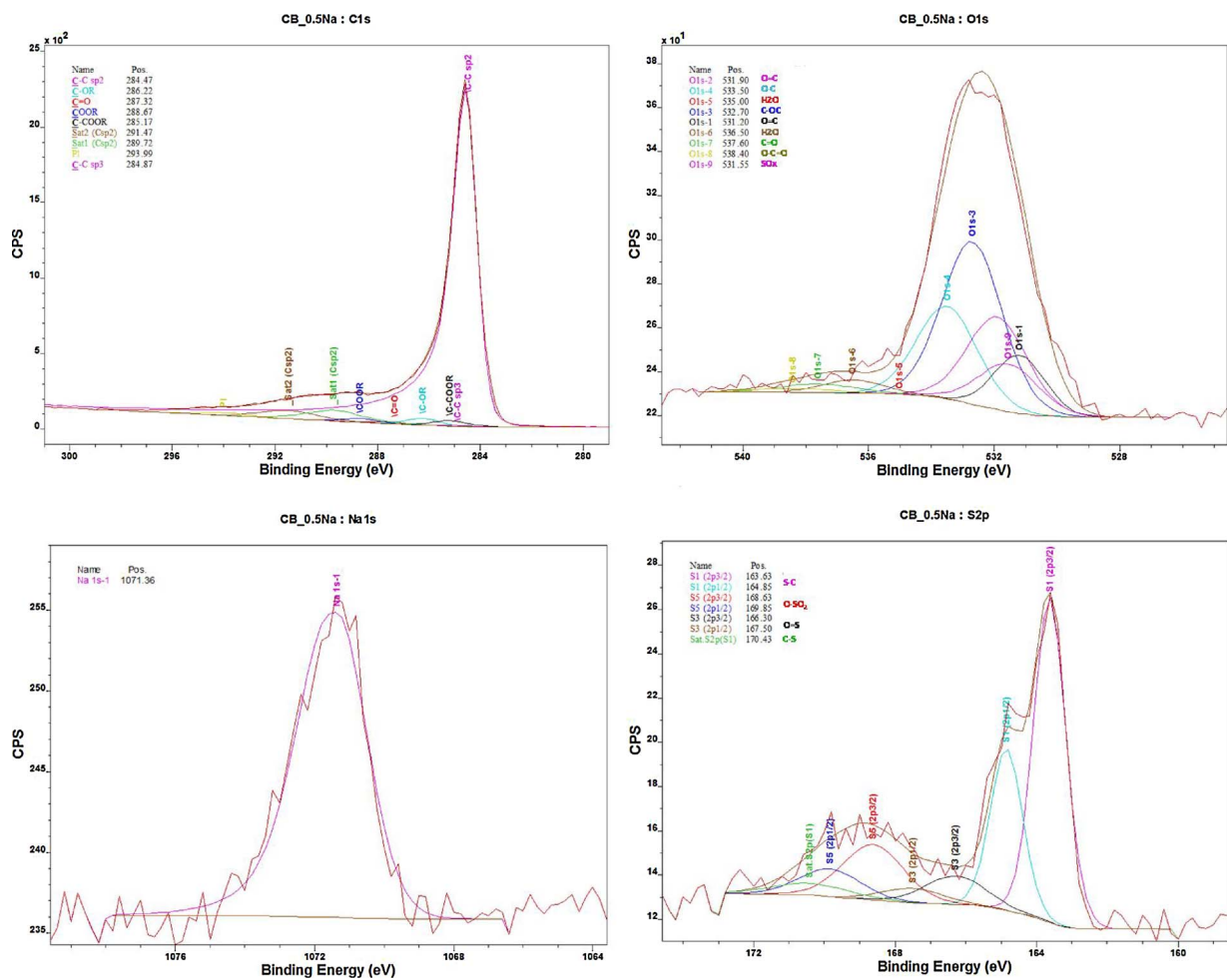


Fig. 1. XP spectra of C1s, O1s, Na1s and S2p of the CB-0,5Na sample.

Finally, as determined by CHONS analyses, no nitrogen was detected with this method. Thus the good decomposition of precursor's salt is also confirmed by XP spectroscopy.

The ratio between the D bands and G band intensities (I_D/I_G) determined with Raman spectroscopy for the doped CB are given in Table 3. G band refers to an ideal graphitic structure while defective bands (D) imply the presence of disordered graphitic lattice (D_1 and D_2) or amorphous carbon (D_3) [24]. Among the entire defective bands D observed, D_1 is the most intense. So the ratio of intensities I_D/I_G is an indicator of structural defects in the material. Table 4 shows that CB-0,5Na and CB-0,5K have higher I_D/I_G ratios than CB350, indicating slightly lower carbon structural order. On the contrary, CB-0,5P is globally more structured. In fact, I_{D2}/I_G and I_{D3}/I_G are decreased in presence of P. The more graphitic structure of CB-0,5P could be attributed to the stabilization of the carbon surface by C—O—P bindings.

The values of surface area (S_{BET}), micropore surface area and micropore volume (V_{micro}) are listed in Table 4. Impregnation of CB by alkali metals significantly increases S_{BET} and V_{micro} . The bulk and surface analyses presented above revealed that CB doped with Na or K have a lower carbon structural order and that bulk to surface Na concentration ratio is equal to 1.9 (Table 2). Based on these considerations, one may conclude that impregnation of CB with alkali metals leads to a modification of the bulk carbonaceous structure with insertion of the metals in the structure, which increases both BET surface area, micropore volume and decreases the degree of organization of the graphitic lattice. On the contrary, doping with P leads to a lower surface specific area. This is attributed to physical blocking of surface sites by phosphate species.

3.2. Soot oxidation under active regeneration conditions

Fig. 3 shows the evolution of the carbon specific oxidation rate during the TGA experiments under air of the CB samples doped by 0.5 wt% of inorganic element.

The activity of the initial model soot sample is significantly modified by the presence of Na, K or P. In fact, alkali metals allow a faster carbon oxidation which further occurs at lower temperatures. The ignition of CB-0,5Na and CB-0,5K takes place 50 °C before the CB350 one. The temperatures at which the maximum oxidation rate (T_{peak}) occurs are also significantly lowered in presence of sodium or potassium respectively by 40 °C (586 °C) and 32 °C (594 °C) compared to the undoped CB350 sample (637 °C). In the temperature range 450 – 500 °C, CB-0,5Na exhibits the highest carbon oxidation rate. The beneficial impact of alkali metal on carbon oxidation by O₂ is in agreement with the literature [11–16]. Phosphorus has the opposite behavior, as it inhibits the carbon oxidation. Such a behavior was already observed on C/C composite, graphite or porous carbons [17–20]. In fact, in presence of P, T_{peak} is shifted to higher temperatures (647 °C) and the total combustion of CB-0,5P is not achieved at 700 °C. Thus, the global reactivity, regarding active regeneration, is as follows: CB-0,5Na > CB-0,5K > CB-0,5P > CB350. The reactivity order of the inorganic elements established here slightly differs from that indicated in the literature, where K shows the best positive impact [14–16]. This difference is linked to the conditions which have been chosen in the present work, as the impact of inorganic elements is compared at a same mass concentration while previous studies consider similar molar concentrations.

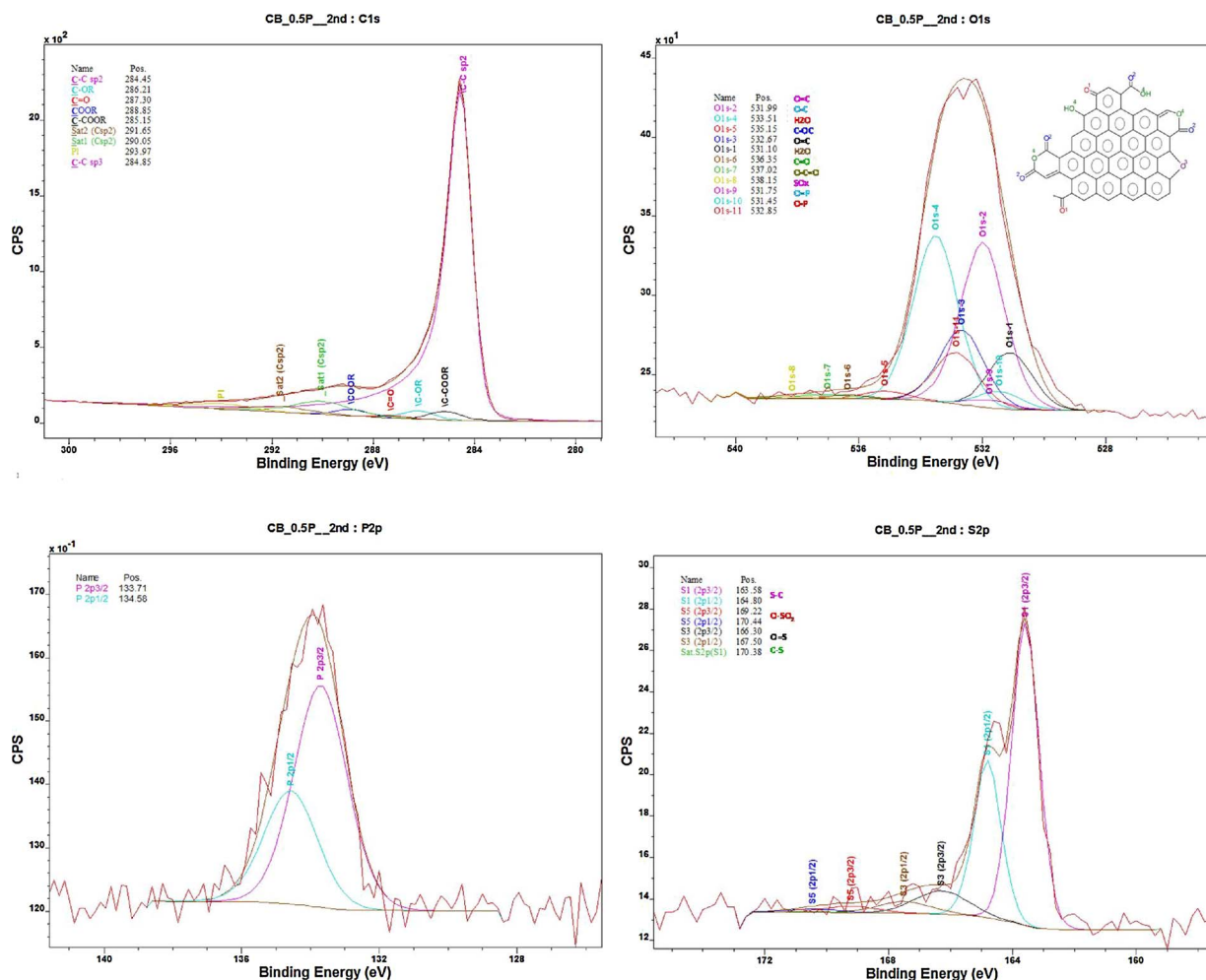


Fig. 2. XP spectra of C1s, O1s, P2p and S2p of the CB-0,5P sample.

Table 2
Elemental composition of the doped carbons black surfaces in wt% determined by XP Spectroscopy.

Sample	C	O	S	Na	P
CB-0,5Na	93,3	5,2	1,3	0,29	/
CB-0,5P	92,4	6,3	0,97	/	0,41

Table 3
I_D/I_G Ratios of doped Carbon Black.

Sample	I _{D1} /I _G	I _{D2} /I _G	I _{D3} /I _G	I _{D4} /I _G
CB350	2.30 ± 0.19	1.03 ± 0.14	0.99 ± 0.11	0.32 ± 0.03
CB-0,5Na	3.12 ± 0.24	1.64 ± 0.38	1.29 ± 0.04	0.44 ± 0.02
CB-0,5K	3.37 ± 0.62	2.06 ± 0.49	1.16 ± 0.31	0.44 ± 0.09
CB-0,5P	2.27 ± 0.19	0.74 ± 0.08	0.28 ± 0.02	1.07 ± 0.17

Table 4
Specific surface area (S_{BET}), microporous pore volume (V_{micro}) of doped Carbon Black.

Sample	S _{BET} (m ² /g _{CB} STP)	Microporous S _{BET} (m ² /g _{CB} STP)	V _{micro} (cm ³ /g _{CB})
CB350	256	117	5.10.10 ⁻²
CB-0,5Na	328	218	9.13.10 ⁻²
CB-0,5K	349	229	9.56.10 ⁻²
CB-0,5P	191	134	5.47.10 ⁻²

3.3. Soot oxidation under passive regeneration conditions

3.3.1. Soot reactivity

The reactivity of the doped CB samples under passive regeneration conditions was evaluated under TPO and under the four gas mixtures containing NO₂. Fig. 4 indicates at which temperature 5% of conversion (T_{5%}) are reached during the oxidation of the samples under the four oxidizing atmospheres. For low conversion, the activity order of the gas mixtures on carbon oxidation (NO₂ < NO₂ + O₂ < NO₂ + H₂O < NO₂ + O₂ + H₂O), already established in previous works [25,26,34], is confirmed with the doped CB samples.

Fig. 5 presents the TPO profiles obtained for the doped CB under NO₂, NO₂ + O₂ and NO₂ + O₂ + H₂O. Whatever the gas mixtures, when they contain NO₂, the ignition temperature of the sample (~200 °C) is lower than under air (~400 °C). This is in agreement with the high oxidizing power of NO₂ [25,26,34].

In presence of only NO₂ (Fig. 5a), the complete oxidation of the sample is not achieved at 700 °C. The impregnation of CB with phosphorus has a small beneficial impact on its reactivity. On the contrary, sodium and potassium significantly increase the carbon specific oxidation rate between 300 and 550 °C.

Fig. 5b presents TPO profiles obtained in presence of NO₂ and O₂ in the gas mixture on the overall temperature range. As it is well known that C-NO₂ reactions are kinetically dominant at low temperatures (< 450 °C), while C-O₂ reaction are the major ones at higher temperatures, results obtained in this study reveal that Na and K enhance both C-NO₂ and C-O₂ reactions. In fact, for temperatures lower than 600 °C, the carbon specific oxidation rates of CB-0,5Na and CB-0,5K are

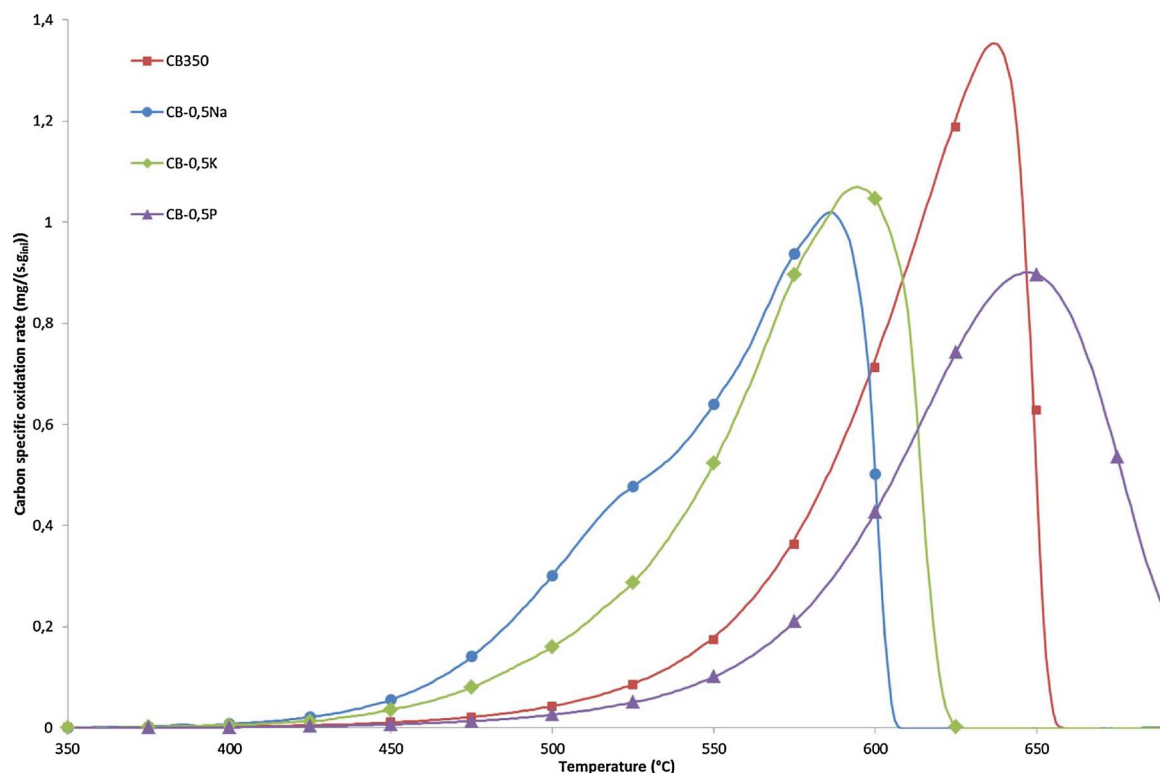
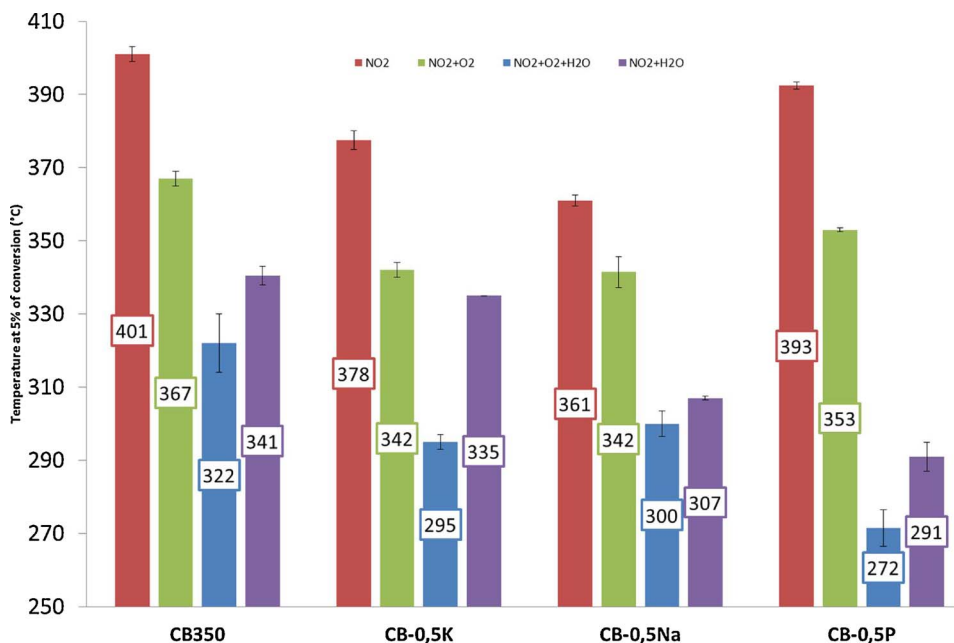


Fig. 3. TGA profiles of doped carbon black under air.

higher than for the CB350 one. The complete combustion of the sample is also achieved at lower temperatures in presence of alkali metals. A shoulder between 425 and 475 °C is visible on the TPO profiles of CB-0,5Na and CB-0,5 K. In presence of P, a little increase in the oxidation rate appears under 500 °C. Beyond this temperature, an inhibition of C-O₂ by phosphorus is found as already observed during TGA experiments (Fig. 3). In fact, the complete oxidation of CB-0,5P is only obtained at 695 °C against 650 °C for CB350.

Finally, the reactivity of doped CB samples was evaluated in presence of water (Fig. 5c). Under NO₂+O₂+H₂O, CB-0,5Na and CB-0,5 K exhibit TPO profiles with a unique main peak around 560 °C, a shoulder

at 500 °C (particularly pronounced with Na) and a small shoulder around 340 °C. The addition of water in the gas mixtures does not impact the beneficial effect of alkali metals on carbon oxidation. Moreover, in presence of water, CB-0,5Na and CB-0,5 K exhibit a very close reactivity. In contrast, the reactivity of CB-0,5P is significantly modified under NO₂+O₂+H₂O. In fact, an inhibition of C-O₂ by P still occurs at high temperatures but, between 200 and 350 °C, CB-0,5P is the most reactive sample. The positive impact of water on the C-NO₂ reaction [25,26,34] seems to be enhanced in presence of phosphorus (Figs. Figure 3 and Figure 5c) as, when H₂O is added to NO₂+O₂, T_{5%} is decreased by around 40 °C for CB-0,5Na, CB-0,5 K and CB350, while it

Fig. 4. Temperature at which 5% of conversion (T_{5%}) is obtained for the doped Carbon Black under several gas mixtures.

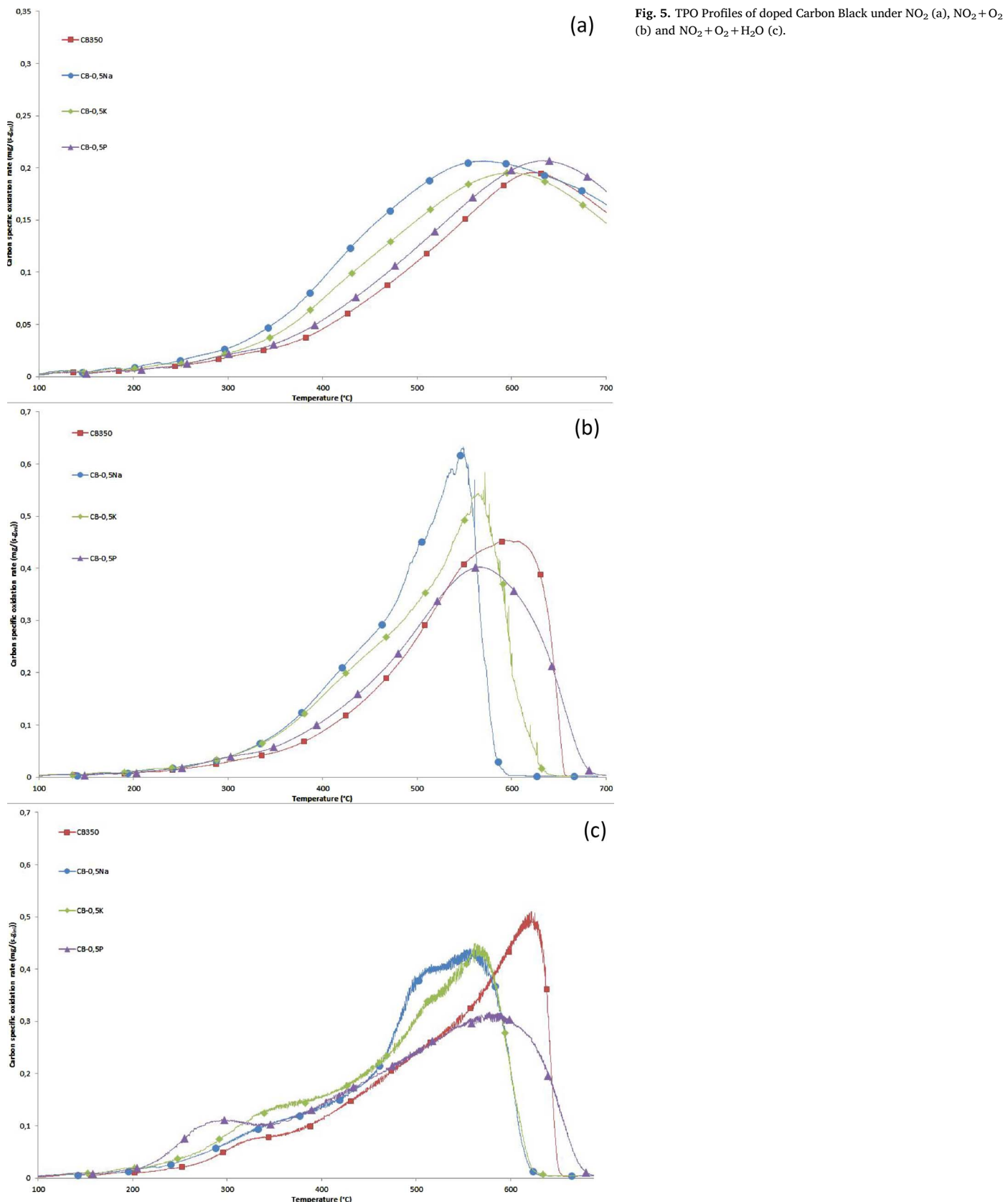


Fig. 5. TPO Profiles of doped Carbon Black under NO_2 (a), $\text{NO}_2 + \text{O}_2$ (b) and $\text{NO}_2 + \text{O}_2 + \text{H}_2\text{O}$ (c).

is decreased by 80 °C for CB-0,5P. Further experiments were performed to verify that this shoulder is reproducible and not linked, for example, to a bad decomposition of the precursor. A raw sample of CB-0,5P was oxidized under $\text{NO}_2 + \text{O}_2 + \text{H}_2\text{O}$ until 365 °C. After cooling under N_2 , the

pre-oxidized sample was submitted to a second TPO under $\text{NO}_2 + \text{O}_2 + \text{H}_2\text{O}$ until complete combustion. Carbon specific oxidation rates measured in this experiment are presented in Fig. 6.

Reactivity of CB-0,5P is the same before and after the treatment.

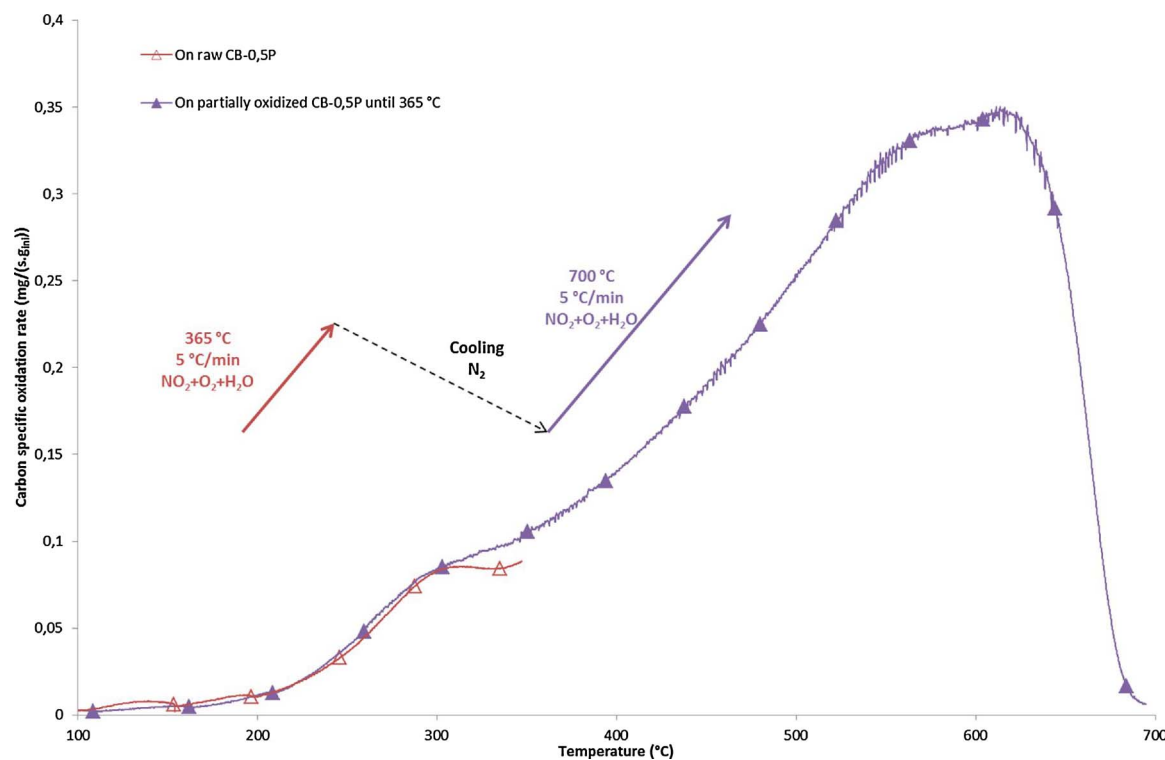


Fig. 6. Oxidizing treatment on CB-0,5P.

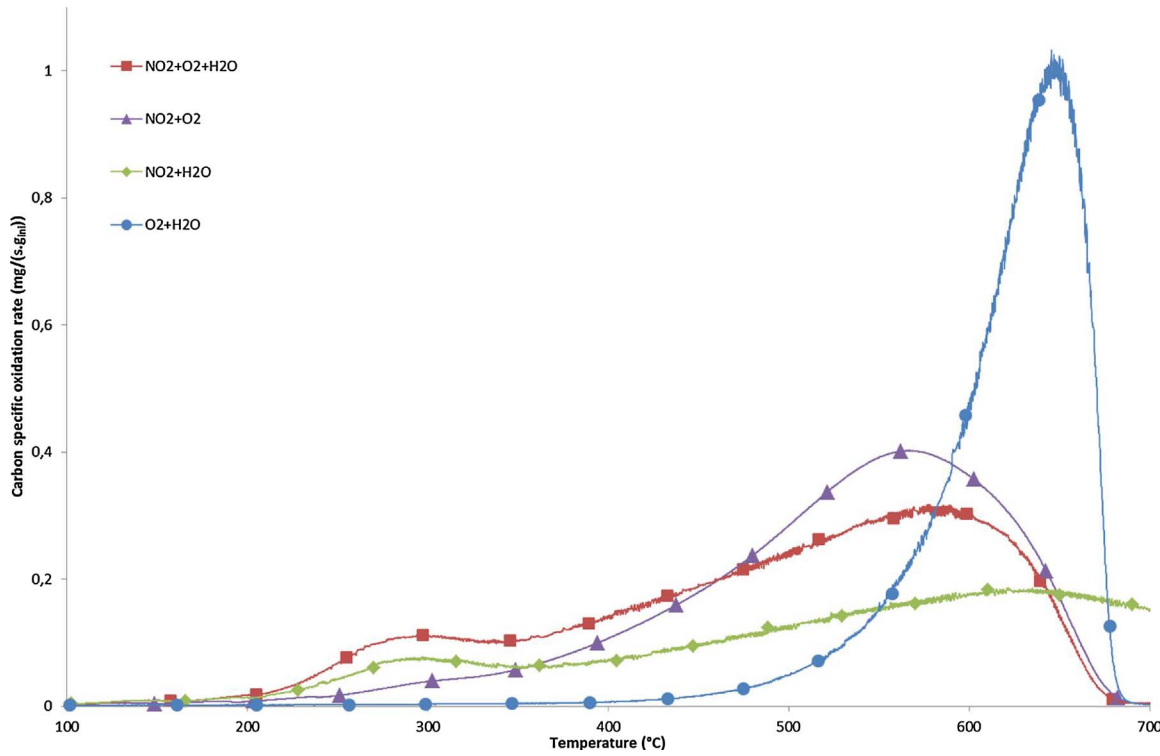


Fig. 7. Impact of gas mixture on CB-0,5P reactivity.

Thus, the phosphorus phase does not evolve in a non-reversible way during TPO experiments and the precursor seems to be well decomposed. The good reproducibility of the shoulder at temperatures lower than 350 °C and the inhibiting effect at high temperatures (> 450 °C) suggest that no loss of P occurs during TPO experiments. The beneficial effect observed in presence of phosphorus at low temperatures with H₂O in the feed gas is thus attributed to a catalytic effect. To determine

if P interacts with C, NO₂ and H₂O or just with C and H₂O, TPO experiments of CB-0,5P under several mixtures were performed. Fig. 7 shows the reactivity of CB-0,5P under NO₂+O₂+H₂O, NO₂+H₂O, O₂+H₂O and NO₂+O₂. The catalytic effect of P on carbon oxidation at low temperature is only observed in the simultaneous presence of NO₂ and H₂O in the gas effluent. No direct reaction between P and water seems to occur.

Table 5

Q ratios at different temperatures for doped Carbon Black samples under NO₂.

Sample	T = 250 °C	T = 300 °C	T = 350 °C	T = 400 °C	T = 450 °C
CB350	0.8	0.9	1.0	1.0	1.1
CB-0,5Na	0.9	0.9	1.0	1.1	1.1
CB-0,5K	0.8	1.0	1.0	1.1	1.1
CB-0,5P	0.8	1.0	1.0	1.1	1.1

3.4. Impact of inorganic elements on the carbon oxidation mechanism

In a gas mixture only containing NO₂, the carbon oxidation takes place through the direct C-NO₂ reaction (reactions 5 and 6) [25,26].



When there is no other oxidation mechanism, the Q ratio defined through

$$Q = \frac{2[CO_2] + [CO]}{[NO]} \quad (7)$$

is equal to 1. But, studying the carbon oxidation under isothermal conditions, between 300 and 400 °C, and under 400 ppmv of NO₂, some authors obtained Q ratios lying between 0.9 and 1.1 [25,35].

Table 5 gathers Q ratio values determined for CB doped with 0.5 wt % of an inorganic element.

Q ratios were calculated from gas emissions measured from TPO experiments under NO₂. The Q ratios were calculated for temperatures between 250 and 450 °C, corresponding to passive regeneration conditions. During the oxidation of CB350 in the temperature range 300 – 450 °C, the Q ratios lie between 0.9 and 1.1, which suggests that the carbon oxidation mechanism, with NO₂ in the feed gas, is not modified in the presence of Na, K or P and so proceeds according to the direct C-NO₂ reactions. The beneficial impact of these elements on carbon oxidation may thus be associated to a catalytic effect, as already proposed by Gross et al. [13]. Similar behaviors are observed under NO₂ + H₂O (not shown here). So the high increase in the oxidation rate observed in presence of NO₂ and H₂O for CB-0,5P is also just a catalytic effect and not a modification of the mechanism.

The addition of an excess of O₂ to NO₂ in the reactive gas flow implies, at temperatures lower than 450 °C, the participation of co-operative reactions involving, simultaneously, O₂ and NO₂ which may be written as follows [35]:



Co-operative reactions take place simultaneously to the direct ones. The occurrence of the co-operative reactions must lead to a change in the relationship between the evolved species CO₂ and NO [35]. Table 6 presents the [CO₂]/[NO] ratio measured for the samples at different temperatures.

It is seen that experimental values are close to 0.5 at 300 °C regardless the CB samples, indicating that only direct C-NO₂ reaction

Table 6

[CO₂]/[NO] ratios at different temperatures for doped Carbon Black samples under NO₂ + O₂.

Sample	T = 300 °C	T = 350 °C	T = 400 °C	T = 450 °C
CB350	0.49	0.55	0.62	0.70
CB-0,5Na	0.53	0.59	0.68	0.77
CB-0,5K	0.54	0.6	0.68	0.76
CB-0,5P	0.49	0.51	0.56	0.61

occurs at this temperature. [CO₂]/[NO] ratio progressively increases with temperature up to a maximum of 0.77, pointing the contribution of both the direct and the co-operative oxidation reactions with a growing participation of the C-NO₂-O₂ reaction. In presence of alkali metals, slightly higher ratios are obtained. These higher [CO₂]/[NO] ratios reveal an enhancement of surface carbon oxygenated complex which are known to be intermediate species able to react with NO₂. Characterizations of CB-0,5Na and CB-0,5 K showed that the impregnation by Na and K leads to an increase in the specific surface area and the oxygen content and a decrease in the degree of organization the graphite sheets. Comparison of XP Spectra of the O1 s energy region of the CB-0,5Na and CB-0,5P samples (Figs. 1 and 2) reveals that, in the CB-0,5Na sample, the major oxidation state of oxygen at the surface is representative of C-OC species while O=C and O-C are dominant for CB-0,5P sample. These structural modifications can explain the increase in active surface carbon oxygenated complex and consequently the better reactivity of CB-0,5Na and CB-0,5 K, regardless the gas mixture composition. Moreover, previous studies attributed a catalytic effect of alkali metal on C-O₂ reaction to their high mobility and their capacity to facilitate oxygen transfer [12–14,16,36–38]. Such a catalytic effect also contributes to an increase in surface -C(O) species. In a similar way, alkali metals can be considered as NO₂ transporters on the carbon surface.

The well-known catalytic effect of water on carbon oxidation is commonly attributed to the formation of nitric and nitrous acid (HNO₃ and HNO₂) [25,35,39]. These acids can react with the carbon surface to form –C(ONO₂) and –C(ONO) complex whose decomposition builds CO₂ and CO. Phosphorus has shown a catalytic effect in the simultaneous presence of NO₂ and H₂O. This beneficial effect can be attributed to the formation of phosphoric acid on the carbon surface which acts in a similar way as nitric acid. On the other hand, TPO presented in this study revealed that P inhibits C-O₂ reaction. Characterizations of CB-0,5P sample showed the presence of surface phosphate species and a decrease in the specific surface area. The inhibiting effect of P on C-O₂ is also attributed to a stabilization of the carbon surface towards the formation of C-O-P bindings and a physical blocking of surface active sites, as proposed in the literature [17–20].

3.5. Modelling the oxidation mechanism

As it is established that the carbon oxidation mechanism is not modified in presence of inorganic elements, the same model can be applied to each sample doped with 0.5 wt% of inorganic element in order to extract the values of the kinetic constants. Figs. 8 and 9 show the evolution during time of, respectively, the mass of carbon and NO₂ emissions for the experimental data (blue) and the simulated data (orange) for doped and non-doped CB in the temperature range 200 °C to 450 °C in which direct and co-operative reactions occur. A good correlation between experimental and simulated data is obtained for all the samples. The model thus describes in a satisfying way the carbon oxidation in presence or not of inorganic elements in TPO conditions.

The pre-exponential factors (A) and activation energies (Ea) calculated for the TPO under NO₂ and NO₂ + O₂ are given in Table 7 for the different samples.

For each sample, the activation energies obtained for the C-NO₂ reactions (Ea_{CO2} and Ea_{CO}) are in the same order of magnitude than the ones which are given in the literature [25,27,34][25,27,34,40]. These energies are also distinctly lower than the ones given for the C-O₂ reaction (160–200 kJ/mol) [26].

Under a gas flow composed only of NO₂ as oxidizing reagent, the four samples show activation energies of the same order of magnitude both for the predominant reaction, forming CO₂, and for the reaction giving rise to the formation of CO. The impregnation of CB by inorganic compounds, however, leads to an increase in the pre-exponential factors, particularly for the reaction (5) leading to the formation of CO₂ (A_{CO2}). The presence of alkali metals has a significant impact on this

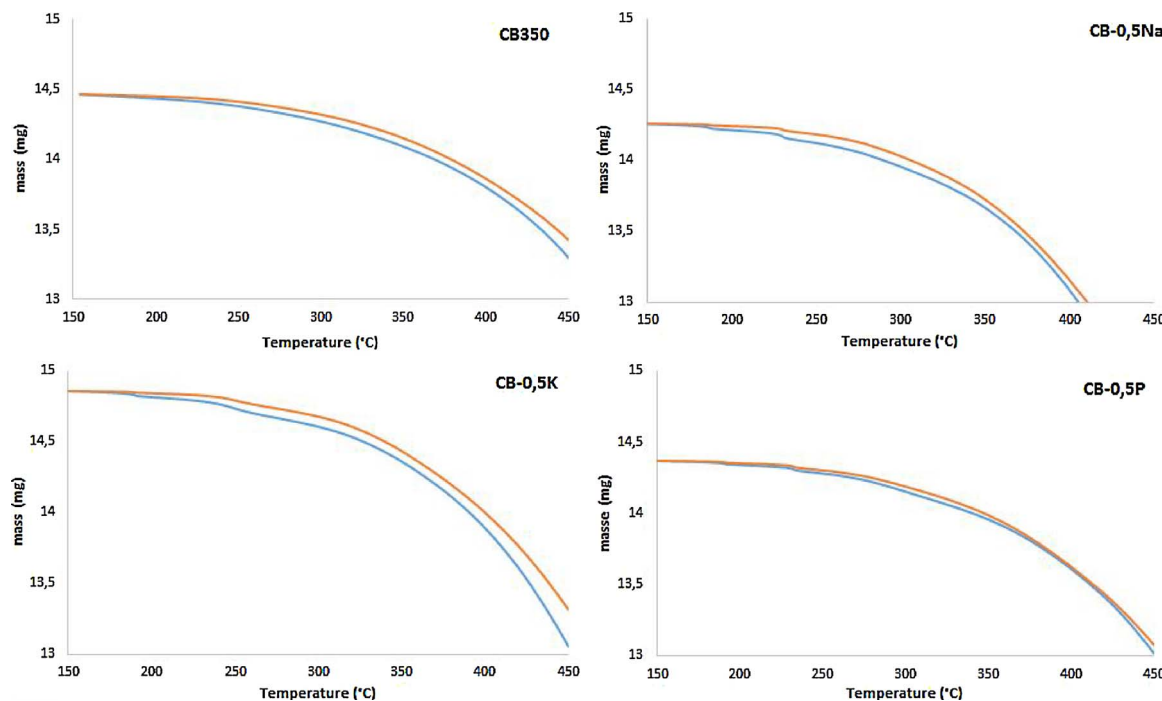


Fig. 8. Mass loss evolution in function of the time during TPO under NO_2 of doped and non-doped CB: blue – experimental data/orange – simulated data. (For interpretation of the references to colour in this figure legend, the reader is referred to the web version of this article.)

term as, compared to CB350 sample, it is multiplied by a factor 8 and 20 for CB-0,5 K and CB-0,5Na samples respectively, while in presence of phosphorus, A_{CO_2} , increases by a factor 1.7 only. Concerning the reaction producing CO, impregnation of CB by inorganic compounds has a lesser impact on the pre-exponential factor (A_{CO}). Thus, the increase in the carbon specific oxidation rate experimentally observed with CB-0,5Na and CB-0,5 K samples, and in a lesser extent with CB-0,5P sample, is linked to a greater number of active sites. Moreover, determination of the kinetic constants reveals that alkali metals have an

effect on both direct reactions (5 and 6), while phosphorus seems to have more impact on the reaction giving rise to the formation of CO.

The activation energies obtained for the $\text{C}-\text{O}_2-\text{NO}_2$ reaction ($E_{\text{aO}_2\text{CO}_2}$ and $E_{\text{aO}_2\text{CO}}$) are in the same order of magnitude than the ones obtained by Jacquot et al. [25]. As for $\text{C}-\text{NO}_2$ reaction, the impregnation by Na or K seems to favor the preponderant reaction (reaction 8). An increase in the pre-exponential factors $A_{\text{O}_2\text{CO}_2}$ is obtained. Concerning CB-0,5Na sample, $A_{\text{O}_2\text{CO}_2}$ is particularly important (multiplied by a factor 6000) which allows to counteract the significant increase in activation energy

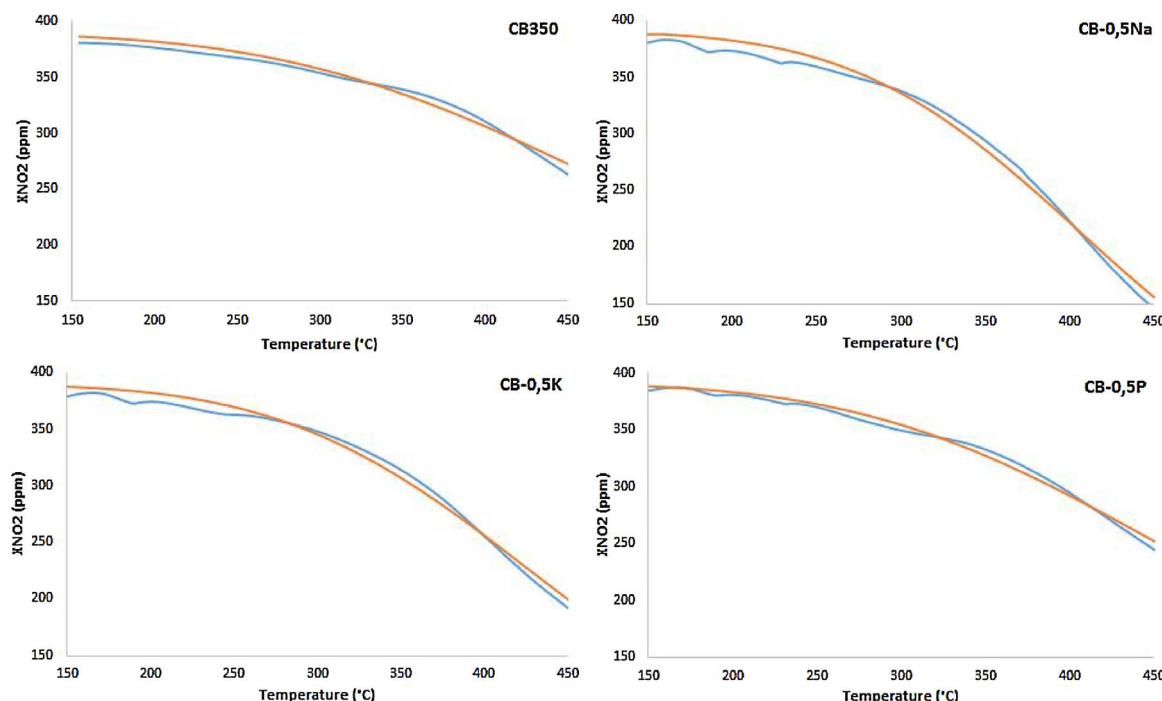


Fig. 9. NO_2 emissions evolution in function of the time during TPO under NO_2 of doped and non-doped CB: blue – experimental data/orange – simulated data. (For interpretation of the references to colour in this figure legend, the reader is referred to the web version of this article.)

Table 7

Kinetic parameters determined by the model for the doped CB samples (k is calculated for $T = 400$ °C).

Sample	CB350	CB-0,5Na	CB-0,5 K	CB-0,5P
A_{CO_2} (Pa $^{-1}$ s $^{-1}$)	3.39.10 $^{-4}$	6.84.10 $^{-3}$	2.65.10 $^{-3}$	5.61.10 $^{-4}$
E_{CO_2} (kJ/mol)	33	45	41	35
$k_{CO_2}^{400}$ (Pa $^{-1}$ s $^{-1}$)	8.94.10 $^{-7}$	2.36.10 $^{-6}$	1.64.10 $^{-6}$	1.04.10 $^{-6}$
A_{CO} (Pa $^{-1}$ s $^{-1}$)	3.75.10 $^{-4}$	5.66.10 $^{-4}$	2.98.10 $^{-4}$	5.65.10 $^{-4}$
E_{CO} (kJ/mol)	42	42	42	41
k_{CO}^{400} (Pa $^{-1}$ s $^{-1}$)	2.23.10 $^{-7}$	2.94.10 $^{-7}$	1.71.10 $^{-7}$	3.75.10 $^{-7}$
$A_{O_2CO_2}$ (Pa $^{-1}$ s $^{-1}$)	3.80.10 $^{-1}$	2.28.10 3	2.21.10 1	2.62.10 $^{-2}$
$E_{O_2CO_2}$ (kJ/mol)	71	113	86	51
$k_{O_2CO_2}^{400}$ (Pa $^{-1}$ s $^{-1}$)	1.10.10 $^{-6}$	4.13.10 $^{-6}$	4.99.10 $^{-6}$	3.06.10 $^{-6}$
A_{O_2CO} (Pa $^{-1}$ s $^{-1}$)	5.63.10 $^{-1}$	7.45	1.44	6.72
E_{O_2CO} (kJ/mol)	75	84	74	88
$k_{O_2CO}^{400}$ (Pa $^{-1}$ s $^{-1}$)	8.06.10 $^{-7}$	2.28.10 $^{-6}$	2.29.10 $^{-6}$	1.06.10 $^{-6}$

$E_{O_2CO_2}$. Impregnation of CB by phosphorus leads to a decrease in both $E_{O_2CO_2}$ and $A_{O_2CO_2}$. Globally, impregnation of CB by inorganic compounds increases the rate of CO_2 formation by the co-operative reaction (8) in the temperature range 150–450 °C. This behavior is more important in the case of alkali metals, and is attributed to the presence of a greater number of active sites. Concerning the reaction producing CO when the feed gas contains O_2 (reaction 9), activation energy E_{O_2CO} are not significantly modified in presence of Na, K or P while the pre-exponential factors A_{O_2CO} increase regardless the sample. The rate of CO formation, as observed for CO_2 , is improved by inorganic elements and especially by alkali metals.

The better reactivity, observed during the TPO under NO_2 and $NO_2 + O_2$, of the CB doped by alkali metals seems to be linked to an increase in the number of active sites of $C-NO_2$ and $C-O_2-NO_2$ reactions. In agreement with the low differences of reactivity observed between CB-0,5P and CB350 below 450 °C during the TPO under NO_2 and $NO_2 + O_2$, the impregnation by P leads to a minor modification of the kinetic parameters of both reactions.

4. Conclusions

Reactivity of Carbon Black impregnated by Na, K or P under a reactive gas flow composed of NO_2 was studied. Surface and structure analysis of CB doped with alkali metals leads to an increase in the specific surface area and the oxygen content and a decrease in the degree of organization the graphite sheets. XPS analysis proved that Na and K are present on the carbon surface in the form M_2SO_x (with $M = Na$ or K and $x = 3$ or 4), TPO experiments revealed that these elements have a beneficial impact on both active and passive regenerations, increasing the number of surface carbon oxygenated active complex of the reaction.

CB doping with P presents a lower specific surface area. Phosphorus is present under phosphate form linked to the carbon surface by C-O-P bindings. This element inhibits carbon oxidation by O_2 beyond 500 °C. On the contrary, P presents, at low temperature (200–450 °C) a catalytic effect on $C-NO_2$ reaction when the gas mixture contains water.

Thus the utilization of Biodiesel, through the presence of inorganic elements, has a beneficial impact on the DPF operating. Further, as passive regeneration is catalyzed, clogging of the filter is limited.

Acknowledgment

The authors gratefully acknowledge the French National Agency for Research for its financial support (Appibio Project, Ref. ANR-14-CE22-0003).

References

- [1] Directive 2009/28/CE du Parlement Européen et du Conseil, (2009).
- [2] Direction générale des Infrastructures, des Transports et de la Mer – Des véhicules aux normes pour réduire la pollution de l'air., (2011).
- [3] A.K. Agarwal, T. Gupta, P.C. Shukla, A. Dhar, Particulate emissions from biodiesel fuelled CI engines, Energy Convers. Manag. 94 (2015) 311–330, <http://dx.doi.org/10.1016/j.enconman.2014.12.094>.
- [4] J. Xue, T.E. Grift, A.C. Hansen, Effect of biodiesel on engine performances and emissions, Renew. Sustain. Energy Rev. 15 (2011) 1098–1116, <http://dx.doi.org/10.1016/j.rser.2010.11.016>.
- [5] P.C. Shukla, T. Gupta, N.K. Labhsetwar, A.K. Agarwal, Trace metals and ions in particulates emitted by biodiesel fuelled engine, Fuel 188 (2017) 603–609, <http://dx.doi.org/10.1016/j.fuel.2016.10.059>.
- [6] Texte de norme EN 14214: 2008, (n.d.).
- [7] D.W. Brookshear, K. Nguyen, T.J. Toops, B.G. Bunting, W.F. Rohr, J. Howe, Investigation of the effects of biodiesel-based Na on emissions control components, Catal. Today 184 (2012) 205–218, <http://dx.doi.org/10.1016/j.cattod.2011.12.001>.
- [8] J. Schobing, V. Tschamber, J.F. Brilhac, A. Auclaire, R. Vonarb, Investigation of the impact of calcium, zinc and phosphorus on DeNOx, Top. Catal. 59 (2016) 1013–1019, <http://dx.doi.org/10.1007/s11244-016-0583-1>.
- [9] A. Lati, A. Spiteri, P. Dimopoulos Eggenschwiler, N. Vogel-Schäuble, Microscopic investigation of soot and ash particulate matter derived from biofuel and diesel: implications for the reactivity of soot, J. Nanoparticle Res. (2012) <http://link.springer.com/article/10.1007/s11051-012-1224-7> . (Accessed 28 November 2016).
- [10] F.-E. López Suárez, A. Bueno-López, M.-J. Illán-Gómez, B. Ura, J. Trawczyński, Study of the uncatalyzed and catalyzed combustion of diesel and biodiesel soot, Catal. Today 176 (2011) 182–186, <http://dx.doi.org/10.1016/j.cattod.2010.11.094>.
- [11] R. Jiménez, X. García, C. Cellier, P. Ruiz, A.L. Gordon, Soot combustion with K/MgO as catalyst, Appl. Catal. Gen. 297 (2006) 125–134, <http://dx.doi.org/10.1016/j.apcata.2005.08.042>.
- [12] R. Jiménez, X. García, C. Cellier, P. Ruiz, A.L. Gordon, Soot combustion with K/MgO as catalyst: II. effect of K-precursor, Appl. Catal. Gen. 314 (2006) 81–88, <http://dx.doi.org/10.1016/j.apcata.2006.08.002>.
- [13] M.S. Gross, M.A. Ulla, C.A. Querini, Catalytic oxidation of diesel soot: new characterization and kinetic evidence related to the reaction mechanism on K/CeO₂ catalyst, Appl. Catal. Gen. 360 (2009) 81–88, <http://dx.doi.org/10.1016/j.apcata.2009.03.011>.
- [14] E. Aneggi, C. de Leitenburg, G. Dolcetti, A. Trovarelli, Diesel soot combustion activity of ceria promoted with alkali metals, Catal. Today 136 (2008) 3–10, <http://dx.doi.org/10.1016/j.cattod.2008.01.002>.
- [15] R. Matarrese, L. Castoldi, L. Lietti, P. Forzatti, Soot combustion: reactivity of alkaline and alkaline earth metal oxides in full contact with soot, Catal. Today 136 (2008) 11–17, <http://dx.doi.org/10.1016/j.cattod.2008.03.022>.
- [16] L. Castoldi, R. Matarrese, L. Lietti, P. Forzatti, Intrinsic reactivity of alkaline and alkaline-earth metal oxide catalysts for oxidation of soot, Appl. Catal. B Environ. 90 (2009) 278–285, <http://dx.doi.org/10.1016/j.apcatb.2009.03.022>.
- [17] M.J. Valero-Romero, F.J. García-Mateos, J. Rodríguez-Mirasol, T. Cordero, Role of surface phosphorus complexes on the oxidation of porous carbons, Fuel Process. Technol. 157 (2017) 116–126, <http://dx.doi.org/10.1016/j.fuproc.2016.11.014>.
- [18] X. Wu, L.R. Radovic, Inhibition of catalytic oxidation of carbon/carbon composites by phosphorus, Carbon 44 (2006) 141–151, <http://dx.doi.org/10.1016/j.carbon.2005.06.038>.
- [19] X. Wu, L.R. Radovic, Catalytic oxidation of carbon/carbon composite materials in the presence of potassium and calcium acetates, Carbon 43 (2005) 333–344, <http://dx.doi.org/10.1016/j.carbon.2004.09.025>.
- [20] D.W. McKee, C.L. Spiro, E.J. Lamby, The inhibition of graphite oxidation by phosphorus additives, Carbon 22 (1984) 285–290, [http://dx.doi.org/10.1016/0008-6223\(84\)90172-6](http://dx.doi.org/10.1016/0008-6223(84)90172-6).
- [21] J. Song, M. Alam, A.L. Boehman, U. Kim, Examination of the oxidation behavior of biodiesel soot, Combust. Flame 146 (2006) 589–604, <http://dx.doi.org/10.1016/j.combustflame.2006.06.010>.
- [22] N. Lamharess, C.-N. Millet, L. Starck, E. Jeudy, J. Lavy, P. Da Costa, Catalysed diesel particulate filter: study of the reactivity of soot arising from biodiesel combustion, Catal. Today 176 (2011) 219–224, <http://dx.doi.org/10.1016/j.cattod.2011.01.011>.
- [23] C.D. Wagner, A.V. Naumkin, A. Kraut-Vass, J.W. Allison, C.J. Powell, J.R.J. Rumble, NIST X-ray Photoelectron Spectroscopy (XPS) Database, Version 3.5, (2003) <https://srdata.nist.gov/xps/> . (Accessed 16 March 2017).
- [24] A. Sadezki, H. Muckenhuber, H. Grothe, R. Niessner, U. Pöschl, Raman microscopy of soot and related carbonaceous materials: spectral analysis and structural information, Carbon 43 (2005) 1731–1742, <http://dx.doi.org/10.1016/j.carbon.2005.02.018>.
- [25] F. Jacquot, V. Logie, J.F. Brilhac, P. Gilot, Kinetics of the oxidation of carbon black by NO₂: Influence of the presence of water and oxygen, Carbon 40 (2002) 335–343, [http://dx.doi.org/10.1016/S0008-6223\(01\)00103-8](http://dx.doi.org/10.1016/S0008-6223(01)00103-8).
- [26] M. Jeguirim, V. Tschamber, J.F. Brilhac, Kinetics of catalyzed and non-catalyzed soot oxidation with nitrogen dioxide under regeneration particle trap conditions, J. Chem. Technol. Biotechnol. 84 (2009) 770–776, <http://dx.doi.org/10.1002/jctb.2110>.
- [27] P. Moreau, P. Valero, A. Brillard, V. Tschamber, J.-F. Brilhac, Y. Hohl, et al., Determination of the Kinetic Parameters for the Soot Combustion Through a Dynamic Numerical Procedure, SAE Tech. Pap. 2015-24-2396, (2015).
- [28] M. Issa, C. Petit, A. Brillard, J.-F. Brilhac, Oxidation of carbon by CeO₂: Effect of the contact between carbon and catalyst particles, Fuel 87 (2008) 740–750, <http://dx.doi.org/10.1016/j.fuel.2007.05.053>.
- [29] D. Briggs, M.P. Seah, Practical Surface Analysis, Auger and X-ray Photoelectron

- Spectroscopy, Wiley, 1990.
- [30] G. Beaman, D. Briggs, High Resolution XPS of Organic Polymers: The Scienta ESCA 300 Database, John Wiley & Sons, 1992.
- [31] A.M. Puziy, O.I. Poddubnaya, R.P. Socha, J. Gurgul, M. Wisniewski, XPS and NMR studies of phosphoric acid activated carbons, *Carbon* 46 (2008) 2113–2123, <http://dx.doi.org/10.1016/j.carbon.2008.09.010>.
- [32] J.J. Ternero-Hidalgo, J.M. Rosas, J. Palomo, M.J. Valero-Romero, J. Rodríguez-Mirasol, T. Cordero, Functionalization of activated carbons by HNO₃ treatment: influence of phosphorus surface groups, *Carbon* 101 (2016) 409–419, <http://dx.doi.org/10.1016/j.carbon.2016.02.015>.
- [33] N. Zouaoui, M. Labaki, M. Jeguirim, Diesel soot oxidation by nitrogen dioxide, oxygen and water under engine exhaust conditions: kinetics data related to the reaction mechanism, *Comptes Rendus Chim.* 17 (2014) 672–680, <http://dx.doi.org/10.1016/j.crci.2013.09.004>.
- [34] M. Jeguirim, V. Tscharner, J.F. Brilhac, P. Ehrburger, Oxidation mechanism of carbon black by NO₂: Effect of water vapour, *Fuel* 84 (2005) 1949–1956, <http://dx.doi.org/10.1016/j.fuel.2005.03.026>.
- [35] L. Zhu, X. Wang, Improving Ce0.5Zr0.5O₂ soot combustion catalysts by KNO₃ loading, *React. Kinet. Mech. Catal.* 112 (2014) 383–395, <http://dx.doi.org/10.1007/s11144-014-0705-3>.
- [36] M. Ogura, R. Kimura, H. Ushiyama, F. Nikaido, K. Yamashita, T. Okubo, Carbonate-promoted catalytic activity of potassium cations for soot combustion by gaseous oxygen, *ChemCatChem* 6 (2014) 479–484, <http://dx.doi.org/10.1002/cctc.201300736>.
- [37] Q. Li, X. Wang, Y. Xin, Z. Zhang, Y. Zhang, C. Hao, et al., A unified intermediate and mechanism for soot combustion on potassium-supported oxides, *Sci. Rep.* 4 (2014) 4725, <http://dx.doi.org/10.1038/srep04725>.
- [38] A.R. Chughtai, W.F. Welch, D.M. Smith, A spectroscopic and gravimetric study of the soot-NO₂N₂O₄ reaction at various temperatures, *Carbon* 28 (1990) 411–421, [http://dx.doi.org/10.1016/0008-6223\(90\)90015-Q](http://dx.doi.org/10.1016/0008-6223(90)90015-Q).
- [39] A. Setiabudi, B.A.L. van Setten, M. Makkee, J.A. Moulijn, The influence of NO_x on soot oxidation rate: molten salt versus platinum, *Appl. Catal. B Environ.* 35 (2002) 159–166, [http://dx.doi.org/10.1016/S0926-3373\(01\)00251-X](http://dx.doi.org/10.1016/S0926-3373(01)00251-X).